PCCP

PAPER

View Article Online
View Journal | View Issue

Cite this: *Phys. Chem. Chem. Phys.*, 2017, **19**, 14114

CO_2 adsorption on different organo-modified SBA-15 silicas: a multidisciplinary study on the effects of basic surface groups†

G. Gatti,*[a] D. Costenaro,[a] C. Vittoni,[a] G. Paul,[a] V. Crocellà,[b] E. Mangano,[c] S. Brandani,[c] S. Bordiga,[b] M. Cossi,[a] L. Marchese[a] and C. Bisio*[ad]

Received 24th November 2016,
Accepted 4th May 2017

DOI: 10.1039/c6cp08048k

rsc.li/pccp

Hybrid organic–inorganic SBA-15 silicas functionalized with increasing amounts of amino groups were studied in this work aiming to evaluate the effects of their physico-chemical properties on CO_2 capture ability. Three different amino-silane species were used: 3-aminopropyltriethoxysilane (APTS), 3-(2-aminoethyl)-aminopropyltrimethoxysilane (EAPTS) and 3-[2-(2-aminoethyl)aminoethyl] aminopropyltrimethoxysilane (PAPTS). More specifically, samples were prepared by using two methods, following a post-synthesis grafting procedure and a one-pot preparation method. Experimental and computational techniques were used to study the structural and textural properties of the obtained samples and their surface species in relation to the adopted preparation method. For the most reactive samples, additional hints on the interactions of organosilane species with the silica surface were obtained by a combination of IR and SS-NMR spectroscopy, with particular emphasis on the effects of the silane chain length on the mobility of the organic species. Advanced complementary solid-state NMR techniques provided deeper information on the interactions of organosilane species with the silica surface. Finally, the amount of CO_2 adsorbed was estimated by comparing the classical microcalorimetric analysis method with a new type of screening test, the Zero Length Column analysis, which is able to evaluate small amounts of samples in a very short time and the adsorption properties of the adsorbents. The reactivity of the amino-modified silica samples is deeply influenced by both the preparation route and by the type of organosilane used for the functionalization of the materials. In particular, samples prepared by the post-synthesis grafting procedure and containing higher amount of amino groups in the chain are more reactive, following the order PAPTS > EAPTS > APTS.

Introduction

In recent decades, the atmospheric concentration of CO_2 has largely increased in relation to anthropogenic causes thus contributing to the global warming (Greenhouse Effect). In order to reduce the amount of CO_2 released to the atmosphere, several methods of Carbon Capture and Storage (CCS) have been proposed in the literature.[1] Three main categories of CO_2 capture technologies include: (i) post-combustion, (ii) pre-combustion, and (iii) oxy-fuel combustion methods. In this respect, the most mature, green and cheap methods are based on post-combustion CO_2 capture processes.[2] Among the available methods, CO_2 wet absorption (*i.e.* liquid phase absorption in amine solutions) is currently one of the most used technologies, although it presents several disadvantages such as the large amount of energy requested for the regeneration, corrosion of the apparatus and volatility of the employed solutions.[3] In order to overcome these problems, a promising approach that has attracted great attention is the CO_2 capture using solid sorbents. This technology seems to be associated with positive environmental effects and energy efficiency.[4]

Several types of solid sorbents have been proposed. In particular, materials working through physisorption (*i.e.* zeolites, activated carbon, MOFs and porous polymers as COFs, CTFs and PAFs) or chemisorption processes (*i.e.* lithium/sodium/potassium based sorbents, calcium oxides, hydrotalcites or amine supported materials) are currently studied.[5–9] Among these materials, organic–inorganic hybrid samples show potential applications

[a] *Dipartimento di Scienze e Innovazione Tecnologica and "Centro interdisciplinare Nano-SiSTeMI", Università del Piemonte Orientale, via T. Michel 11, 15121 Alessandria, Italy. E-mail: giorgio.gatti@uniupo.it, chiara.bisio@uniupo.it*
[b] *Dipartimento di Chimica, NIS, INSTM Reference Centre, Università di Torino, Via Quarello 15/A, 10135 Torino, Italy*
[c] *Scottish Carbon Capture and Storage, School of Engineering, University of Edinburgh, Mayfield Road, Edinburgh, EH9 3JL, UK*
[d] *ISTM-CRN Istituto di Scienze e Tecnologie Molecolari, via G. Venezian 21, Milano, Italy*

† Electronic supplementary information (ESI) available. See DOI: 10.1039/c6cp08048k

as CO_2 adsorbents, owing to their high adsorption capacity, high selectivity, and excellent chemical stability.[1] Among these porous solids functionalized with amino groups deserve particular attention in relation to the encouraging results. These materials can be prepared by incorporation of different organic compounds containing amino groups (*i.e.* through grafting of aminosilanes or impregnation of monomers and polymers as polyethylenimine[10]) on the surface of the supporting materials.[11]

As a general feature, the interaction of CO_2 with primary and secondary amines leads to the formation of carbamates and carbamic acid species.[12] It is proposed in many publications that the reaction is governed by several different mechanisms.[13,14] At first, the terminal amino group of the alkyl chain can react with the CO_2 forming a zwitterionic intermediate (a). The following two ways are possible for the zwitterionic intermediate: (i) a rearrangement with the consequent formation of carbamic acid (b1); (ii) an interaction with a free base such as water, hydroxyl groups of silanols or another amine, forming an alkylammonium carbamate species (b2).

$$\text{R-NH}_2 + \text{CO}_2 \rightarrow \text{R-NH}_2^+\text{COO}^- \quad \text{(a)}$$

$$\text{R-NH}_2 + \text{COO}^- \rightarrow \text{R-NHCOOH} \quad \text{(b1)}$$

$$\text{R-NH}_2 + \text{COO}^- + \text{Base} \rightarrow \text{R-NHCOO}^- + \text{BH}^+ \quad \text{(b2)}$$

Under dry conditions, if the organic chain contains only one amino group, the reaction takes place *via* the intermolecular mechanism. This involves an amine group of another molecule, if the silane density is high and the organic chains are close enough, or a silanol group of the silica surface. If, on the other hand, the alkyl chain contains another amino group, the base B is present in the same molecule, and therefore the reaction can also occur *via* the intramolecular mechanism.[15]

Ordered porous silica-based materials like HMS, mesoporous silica microspheres, mesocellular silica foam, MCM-41, MCM-48, SBA-12, SBA-15, SBA-16 and KIT-6, have been widely investigated as solid sorbents for CO_2 capture.[11] In fact, they are good candidates for CO_2 capture due to their structural and textural properties, such as large pore size, high specific surface area and pore volume. All these properties facilitate a good dispersion of basic amino groups on the surface, thus increasing CO_2 adsorption capacity.[16]

Compared to the other mesoporous materials, SBA-15 was found to be one of the most suitable substrates for CO_2 capture thanks to its large pore volume and diameter.[5] Additionally, the intra-wall pores of SBA-15 form a continuous network that connects adjacent channels, which promotes the mass transfer during adsorption. This facilitates the interaction between the CO_2 and the amino groups and results in the formation of carbamate groups.[17]

Different studies of CO_2 adsorption on SBA-15 silica containing amino species are reported in the literature. For example, Wang *et al.*[3] grafted SBA-15 silica with 3-aminopropyltrimethoxysilane obtaining a material with CO_2 uptake of *ca.* 1.59 mol kg^{-1} at 25 °C and 0.15 atm, while Chang *et al.*[18] used 3-trimethoxysilylpropyl diethylenetriamine as a grafting agent that exhibited a CO_2 adsorption capacity of a 2.41 mol kg^{-1} adsorbent, (60 °C, 0.15 atm).

Even though several studies in the literature have reported the use of silanes with different concentrations of basic species, the CO_2 capture performances of these materials are difficult to be compared in that in many cases different conditions of pressure and temperature have been adopted.

Recently, Yoo *et al.*[15] compared SBA-15 functionalized with amine-containing organosilanes with different chain lengths (including 3-aminopropyltrimethoxysilane (APTS), 3-(2-aminoethyl)aminopropyltrimethoxysilane (EAPTS) and 3-[2-(2-aminoethyl)aminoethyl]aminopropyltrimethoxysilane (PAPTS)) with low loading of silane adsorbents (~0.45 mmol silane per g). In their work, particularly focused on the determination of the CO_2 adsorption mechanism with a functionalized silica surface, they suggested the occurrence of an intramolecular mechanism for CO_2 adsorption on EAPTS and PAPTS, whereas for samples grafted with shorter silane species (APTS) an intermolecular mechanism was proposed. The key role of silanol groups in CO_2 interactions was also enlightened.

In our work, hybrid organic–inorganic SBA-15 materials functionalized with high loading of APTS, EAPTS and PAPTS were prepared by using both post-synthesis and one-pot methods, aiming to determine the effect of the synthesis procedure on the CO_2 adsorption processes. It is known indeed that materials prepared using one-pot methods have a more homogenous distribution of organic species and, in general, the amount of incorporated functional species is higher with respect to samples prepared using the post-synthesis method.[19] To our knowledge, SBA-15 related samples functionalized *via* a one-pot procedure with EAPTS and PAPTS were prepared for the first time in this work.

The structure and interactions occurring at the surface of different hybrid organic–inorganic materials were studied by coupling experimental (mainly IR and SS-NMR spectroscopy) and computational techniques. ^{1}H Hahn echo MAS NMR was applied for the first time to provide hints on the interactions between amine and surface silanols, aming to evaluate the mobility of the chains on the SBA-15 surface, a relevant parameter that influences the adsorption performances. *Ab initio* calculations were also considered to determine the structure of the functionalized materials.

Adsorption of CO_2 on the materials was studied by different experimental techniques. Besides classical IR spectroscopy, SS-NMR, microcalorimetric analysis and Zero Length Column chromathography were also used. This last experimental technique is a new quantitative analysis for hybrid organic–inorganic samples, and represents a relevant screening method for prototype adsorbers because it requires small amounts of samples and very short time of analysis.

Experimental

Materials preparation

SBA-15 silica. The SBA-15 mesoporous silica was prepared following the synthesis method reported by Zhao.[20] The Pluronic P123 triblock copolymer (4.0 g, Sigma Aldrich, 435465-250ML, M_W = 5800) was dissolved in 30 mL of deionized water in a

thermostated bath at 35 °C. The obtained gel was mixed using a mechanical stirrer for 24 h; after this, 120 g of 2 M HCl solution was slowly added to the gel. After 1 h, tetraethyl orthosilicate (TEOS) (8.5 g, $Si(OC_2H_5)_4$, Sigma Aldrich, 131903-25ML, M_W = 208.33 g mol^{-1}) was finally added. After 1 h stirring, the gel was introduced in a Teflon autoclave (125 mL capacity, Anton PAAR 4748) and heated at 100 °C for 24 h. At the end of this procedure, the samples were filtered, washed with 2 L of deionized water and dried for 36 h at 120 °C. The material was then calcined under air flow (100 mL min^{-1}) at 550 °C for 5 h (heating ramp 1 °C min^{-1}) in order to remove the organic species used as template molecules.

Post-synthesis functionalization of SBA-15 silica. The bare SBA-15 sample was functionalized in order to introduce amino groups on the surface by using a post-synthesis grafting procedure. Three different organic silanes were used: 3-aminopropyltriethoxysilane (APTS), 3-(2-aminoethyl)aminopropyltrimethoxysilane (EAPTS) and 3-[2-(2-aminoethyl)aminoethyl]aminopropyltrimethoxysilane (PAPTS).

Three aliquots of 1.0 g of SBA-15 silica were treated under vacuum at 200 °C for 2 h to remove physisorbed water. After this treatment, the samples were kept under N_2 flow and then dispersed in 100 mL of anhydrous toluene before the addition of the organic silane. In one case, 0.53 mL of 3-aminopropyltriethoxysilane [(APTS) $(H_2N(CH_2)_3Si(OCH_3)_3$, Sigma-Aldrich, M_W = 221.37 g mol^{-1})] were added drop-by-drop to the SBA-15 suspension that was then left for 20 h at 50 °C under magnetic stirring. After this, the sample was recovered by filtering, and the powder was washed with toluene and ethyl ether to remove the unreacted silane, and finally dried for 1 night at 80 °C.[21] This sample hereafter will be named as A-SBA15. For the other two SBA-15 samples, 0.49 mL of *N*-[3-(trimethoxysilyl)propyl]-ethylenediamine (EAPTS) $(H_2N(CH_2)_2NH(CH_2)_3Si(OCH_3)_3$, Sigma-Aldrich, M_W = 222.36 g mol^{-1}) and 0.48 mL of *N*-[3-(trimethoxysilyl)propyl]-diethylenetriamine (PAPTS) $(H_2N(CH_2)_2NH(CH_2)_2NH(CH_2)_3Si(OCH_3)_3$, Sigma-Aldrich, M_W = 265.43 g mol^{-1}) were added, respectively. The same preparation protocol adopted for A-SBA-15 was followed in the case of these samples. The recovered samples hereafter will be named as E-SBA-15 and P-SBA-15, respectively.

One-pot preparation of functionalized SBA-15 related materials. Organo-modified SBA-15 silica samples were also prepared *via* one-pot synthesis by adapting the method reported by Hao *et al.*[22] In particular, the Pluronic P123 triblock copolymer (2.0 g, Sigma Aldrich, 435465-250ML, M_W = 5800) was dissolved in 15 mL of deionized water in a thermostated bath at 35 °C. The obtained gel was mixed using a mechanical stirrer for 24 h; after this time 60 g of 2 M HCl solution was slowly added to the gel. After 1 h, tetraethyl orthosilicate (TEOS) (3.8 g, $Si(OC_2H_5)_4$, Sigma Aldrich, 131903-25ML, M_W = 208.33 g mol^{-1}) was finally added. After the addition of TEOS the solution was stirred for two hours and then a 10 mol% of the desired organosilane (*i.e.* APTS, EAPTS or PAPTS) was added to the gel and stirred for 24 hours. After this time, the gel was introduced in a Teflon autoclave (125 mL capacity, Anton PAAR 4748) and heated at 100 °C for 24 h. At the end of this procedure, samples were filtered, washed with 2 L of deionized water and dried for 36 h at 120 °C. The organic template was removed by extraction with ethanol at 80 °C for 24 h. Finally, the organo-functionalized silica samples were dried again at 120 °C for 16 hours. The obtained samples will be hereafter named as A-SBA-15(OP), E-SBA-15(OP) and P-SBA-15(OP), respectively.

Characterization techniques

X-ray diffractrograms (XRD) were collected on unoriented ground powders using a Thermo ARL 'XTRA-048 diffractometer with a CuKα (λ = 1.54 Å) radiation, from 0.7 to 3° 2θ degrees with a step size of 0.02° 2θ and a rate of 1° 2θ min^{-1}.

N_2 physisorption measurements were carried out at 77 K in the relative pressure range from 10^{-7} to 1 p/p_0 by using a Quantachrome Autosorb iQ2 instrument. Before the analysis the samples were outgassed at 150 °C for 3 h (residual pressure $p < 10^{-6}$ Torr). Specific surface areas were determined by using the Brunauer–Emmett–Teller equation, in the residual pressure range from 0.01 to 0.1 p/p_0. Pore size distributions were obtained by applying the Non Localized Density Functional Theory (NLDFT) method (N_2 silica kernel based on a cylindrical pore model).

Thermogravimetric analyses (TGA) were performed on a Setaram SETSYS Evolution instrument under O_2 (gas flow rate 100 mL min^{-1}), heating the samples from 30 °C to 800 °C with a rate of 5 °C min^{-1}.

C–H–N elemental contents were determined using an EA 3000 elemental analyser (EuroVector). Helium and oxygen at 120 and 35 kPa pressures were used, respectively. For each material, three measurements were done.

Infrared spectra were collected on a Thermo Electron Corporation FT Nicolet 5700 Spectrometer (resolution 4 cm^{-1}). Self-supporting pellets were placed into a homemade IR cell with KBr windows permanently attached to vacuum line (residual pressure < 1 × 10^{-4} mbar), allowing all treatments and adsorption–desorption experiments to be carried out *in situ*. Before the gas adsorption tests, the silica samples were outgassed at 135 °C with a heating ramp of 5 °C min^{-1} for 3 h; an oil-free apparatus and a grease-free vacuum line were used. The samples were cooled at room temperature for the collection of IR spectra upon CO_2 adsorption. All the spectra were normalized by dividing the density of the self-standing pellets, obtained by dividing the sample mass for the area of the pellets. The sample mass values were 0.0014 g, 0.0021 g and 0.0011 g, while the areas of the pellets were 52 mm^2, 67 mm^2 and 42 mm^2, respectively for A-SBA-15, E-SBA-15 and P-SBA-15. In addition, the proper normalization of the IR spectra was verified taking as reference the intensity of the overtones and combination modes of the silica framework (bands in the 2200–1600 cm^{-1} range). In this way, differences in the band intensities among different samples related to intrinsic oscillators of the materials (*e.g.* hydroxyl groups) can be associated with actual differences in the amount of such species in the samples. As a consequence of the normalization, the absorbance values are reported as the arbitrary unit (a.u.).

Solid state NMR (SS-NMR) spectra were acquired on a Bruker Avance III 500 spectrometer and a wide bore 11.7 Tesla magnet

with operational frequencies for ^{1}H, ^{29}Si and ^{13}C of 500.13, 99.35 and 125.77 MHz, respectively. A 4 mm triple resonance probe with MAS was employed in all the experiments. The samples were packed on a Zirconia rotor and spun at a MAS rate in the 0–15 kHz range. The magnitudes of radio frequency fields, ν_{rf}, were 62.5 and 33.3 kHz for ^{13}C and ^{29}Si, respectively. The relaxation delays, d1, between accumulations were 2.5, 100 and 180 s for ^{1}H, ^{13}C and ^{29}Si MAS NMR, respectively. For the $^{13}C\{^{1}H\}$ CPMAS experiments, the radio frequency fields ν_{rfH} of 55 and 28 kHz were used for initial excitation and decoupling, respectively. During the CP period the ^{1}H RF field ν_{rfH} was ramped using 100 increments, whereas the ^{13}C RF field ν_{rfC} was maintained at a constant level. During the acquisition, the protons are decoupled from the carbons by using a TPPM decoupling scheme. A moderate ramped RF field ν_{rfH} of 62 kHz was used for spin locking, while the carbon RF field ν_{rfC} was matched to obtain the optimal signal and the CP contact time of 2 ms was used. The rotor synchronized Hahn echo sequence ($\pi/2$–τ–π–τ–acquisition) was also applied to record the ^{1}H NMR spectra with a τ delay time of 6700 μs and a 90° pulse length of 2.5 μs. All chemical shifts are reported using the δ scale and are externally referenced to TMS at 0 ppm. All ^{29}Si MAS NMR spectra were fitted with DMFIT functions for quantitative deconvolution of overlapping peaks.[23] Before the gas adsorption tests, the silica samples were outgassed at 135 °C with a heating ramp of 5 °C min^{-1} for 3 h; an oil-free apparatus and a grease-free vacuum line were used. The samples were cooled at room temperature and 60 mbar of $^{13}CO_2$ was placed in contact with the samples and then kept at that atmosphere for at least 2 days. After that the rotor was packed in a glove box and submitted for solid state NMR experiments. The label $^{13}CO_2$ was used in order to increase the signal intensity.

Microcalorimetric CO_2 adsorption measurements to calculate the heat of adsorption were carried out at 30 °C by means of a heatflow microcalorimeter (Calvet C80, Setaram, France) connected to a grease-free high-vacuum gas-volumetric glass apparatus (residual $p \approx 10^{-6}$ Torr) equipped with a Ceramicell 0–100 Torr gauge and a Ceramicell 0–1000 Torr gauge (by Varian), following a well-established stepwise procedure, described in detail elsewhere.[28] This procedure allows, during the same experiment, the determination of both integral heats evolved ($-Q_{int}$) and adsorbed amounts (n_a) for very small increments of the adsorptive pressure. The adsorbed amounts and integral heats evolved, normalized to the sample mass, have been plotted *vs.* pressure in the form of volumetric (quantitative) and calorimetric isotherms (here not reported for the sake of brevity), respectively. The adsorption heats obtained for each small dose of gas admitted over the sample (q_{diff}) have been finally reported as a function of coverage, in order to obtain the (differential) enthalpy changes associated with the proceeding adsorption process ($q_{diff} = -\Delta_{ads}H$). The differential-heat plots presented here were obtained by taking the middle point of the partial molar heats ($\Delta Q_{int}/\Delta n_a$, kJ mol^{-1}) *vs.* n_a histogram relative to the individual adsorptive doses. Before the quantitative/calorimetric measurement, all materials were activated under vacuum at 150 °C for 3 hours. In all experiments, after the first adsorption run carried out on the activated samples (the primary isotherm), samples were outgassed overnight at the adsorption temperature (30 °C), and then a second adsorption run was performed (the secondary isotherm), in order to check whether secondary and primary adsorption runs coincided, or an irreversible adsorbed fraction was present.

The zero length column consists of a 1/8″ Swagelok union in which a very small amount of sample (10–15 mg) is placed as monolayers between two sister discs. The method was originally introduced to measure the intra-particle diffusion of hydrocarbons in zeolites[24] and, more recently it has been extended to the screening of the adsorption properties of novel adsorbents for CO_2 capture.[25,26] The experiment is based on following the desorption curve of a sample previously equilibrated with a known mixture at a constant flow rate. For the characterization of adsorbents for post-combustion capture the feed mixture is composed of 10% CO_2 in He. Once the equilibrium is reached the inlet flow to the ZLC is switched to pure He (carrier) and the desorption starts. The system is equipped with drying columns to ensure the removal of any traces of water from the gases entering the system. The concentration of the gas phase is monitored using a Dycor Ametek Benchtop quadrupole mass spectrometer connected to the outlet of the ZLC. Full details of the system used for these experiments are given in an earlier publication.[26] For this study the amount of sample packed in the ZLC is: SBA-15 (2.4 mg), A-SBA-15 (3.5 mg), E-SBA-15 (5.9 mg), and P-SBA-15 (7.3 mg).

Prior to each experiment the samples were regenerated overnight at 150 °C under He flow. Each experiment was carried out at two different flow rates, 2 and 2.7 mL min^{-1}, to check if the samples are in equilibrium or kinetically controlled.[27] To ensure that complete equilibrium was achieved the ZLC experiment was repeated at increasing adsorption times. The system was considered to be in equilibrium when the CO_2 uptake did not change any more with the adsorption time. According to this procedure the resulting equilibration time for A-SBA-15 was 40 min while for E-SBA-15 and P-SBA-15 the adsorption time required was 20 min.

Theoretical calculations have been performed using the Gaussian09 program at the Density Functional Theory (DFT) level, with the hybrid functional B3LYP[29–31] using Dunning's correlation-consistent cc-PVDZ basis set on light atoms,[32,33] and LANL2DZ effective core potentials and the basis set for silicon.[34] The atom–atom pairwise algorithm proposed by Grimme[35] and implemented in Gaussian09 was used to estimate the contribution from dispersion (van der Waals) forces to energies and geometrical structures.

The silica surface was simulated by two cluster models, with Si39O112H68 (I) and Si52O152H92 (II) stoichiometry: the models have a surface of approximately 2.5 and 4 nm^2, respectively; hydrogen atoms were added to saturate the oxygen valences at the cluster border and on the ''external'' surface. These clusters were extracted from the large model of amorphous silica optimized in the literature,[36] dealing with MCM-14 modeling: though MCM-14 and SBA-15 differ for the mesoscopic structure, *i.e.* mesopore size and channel topology, at this scale the atomistic

structures of their inner surfaces are fully comparable. The silanol concentration on the model surfaces, a crucial parameter to describe the interactions with the attached molecules, was set to 5 SiOH nm^{-2}, to reproduce the experimental measures described below.

To simulate the functionalized surfaces, one to three molecules of APTS, EAPTS and PAPTS were grafted to cluster I and II surfaces by eliminating three water molecules from silanol groups, and thus forming three Si–O–Si bonds per chain; when more than one molecule was added, a homogeneous distribution of chains attached to the surface was assumed.

Results and discussion

Physico-chemical properties of organo-modified SBA-15 silicas

The structural properties of hybrid organic–inorganic SBA-15 samples prepared using post-synthesis grafting and one pot method were studied by XRD analysis (Fig. 1).

The pure SBA-15 silica sample after calcination to remove the polymer template (Fig. 1A) shows reflections at 0.9, 1.5 and 1.8° 2θ, corresponding to the (100), (110) and (200) planes typical of hexagonally ordered mesoporous silica.[20,37] All samples in Fig. 1A show the same reflections indicating that, as expected, the process of grafting did not modify the ordered structure typical of these materials. Diffraction patterns of samples prepared using a one-pot method are reported in Fig. 1B. The A-SBA-15 (OP) sample is characterized by the presence of (100) reflection at *ca.* 0.9° 2θ and a broad signal in the 1.5–2° 2θ range where reflections related to the (110) and (200) planes are probably merged. Samples prepared with silanes with longer chains (*i.e.* EAPTS and PAPTS) appeared to be less organized with respect to A-SBA-15 (OP), as indicated by the presence of single and broad reflection related to the (100) plane. This suggests that the use of silanes with longer chains for the synthesis of mesoporous materials led to a more disordered mesoporous structure. One-pot samples were also studied by TEM in order to have direct information on pores arrangement (Fig. S1 in ESI†).

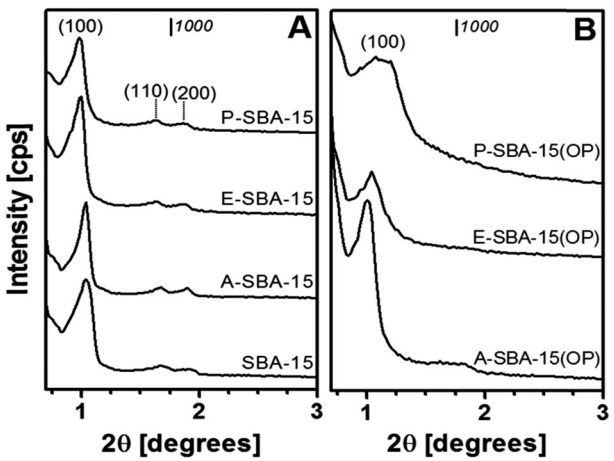

Fig. 1 XRD pattern of the pure SBA-15 material and post-synthesis grafted samples (frame A) and SBA-15 related materials prepared using a one-pot method (frame B).

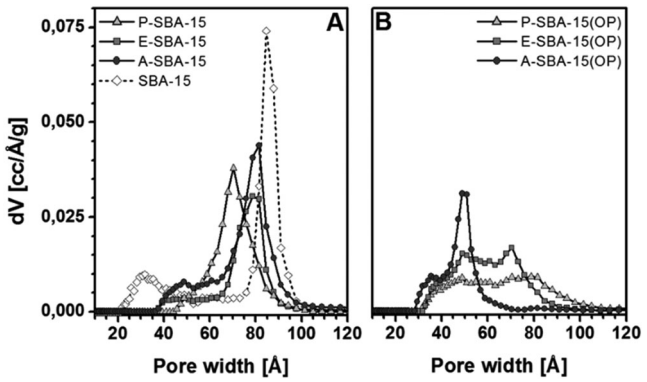

Fig. 2 Pore size distribution (determined by N_2 physisorption at 77 K applying NLDFT methods) of grafted samples compared to the parent SBA-15 material (frame A) and one-pot synthesized materials (frame B).

The A-SBA-15 (OP) and E-SBA-15 (OP) samples are characterized by a well-organized hexagonal arrangement of pores (even if in the latter sample appeared less ordered), whereas the porous architecture of the P-SBA-15 (OP) material is more disordered, in agreement with the XRD analysis.

N_2 physisorption analysis at 77 K was carried out to collect information on the textural properties of the grafted and one-pot prepared samples, with special consideration to the determination of specific surface area and pore size distribution. In particular, pore size distribution of the obtained samples is reported in Fig. 2.

All samples (both prepared by one-pot method and post-synthesis grafting) show type IV adsorption isotherms based on the IUPAC classification, indicating the presence of mesoporosity in the materials. For all grafted samples an H1 hysteresis loop typical of materials with a cylindrical pore can be observed (Fig. S2 in the ESI†).[38] The BET method was used to estimate the specific surface area (S.S.A.) of the solids. The bare SBA-15 silica shows a S.S.A. of 720 $m^2\ g^{-1}$, whereas a progressive decrease of the S.S.A. for the grafted silica samples was observed as a function of the silane chain length: 563, 360 and 236 $m^2\ g^{-1}$ for the samples A-SBA-15, E-SBA-15 and P-SBA-15, respectively (Table 1). The reduction of the specific surface area should be ascribed to the presence of the organic species that limit the entrance to the SBA-15 pores: the longer the silane chain length, the stronger the pore blocking effect.[39] The A-SBA-15(OP) sample is characterized by hysteresis loops of H2a type following new IUPAC definition,[40] suggesting the presence of more disordered pores with respect to the analogous grafted samples. The shape of the isotherm suggested a complex pore architecture in which pore blocking and percolations effects can be postulated (Fig. S2 in the ESI†). Also the E-SBA-15(OP) and P-SBA-15(OP) samples show hysteresis loops of H2a type, thus indicating the presence of materials with disordered pores and larger pores. The specific surface area (S.S.A.) of one-pot prepared samples progressively decrease from A-SBA-15(OP) to P-SBA-15(OP), passing from 552 to 416 $m^2\ g^{-1}$ (Table 1). The pore size distribution of silica samples was determined by the NLDFT model using a kernel based on a cylindrical pore model related to the desorption

Table 1 Specific surface area (S.S.A.), total pore volume (V_p), nitrogen and silane concentrations of both grafted (A-SBA-15, E-SBA-15 and P-SBA-15) and one-pot (A-SBA-15(OP), E-SBA-15(OP) and P-SBA-15(OP)) samples. Pure silica SBA-15 is also reported for comparison

Sample	S. S. A. [$m^2\ g^{-1}$]	V_p [cc per g]	Conc. N^a [mmol g^{-1}]	Conc. silane^b [mmol g^{-1}]
SBA-15	720	0.98	—	—
A-SBA-15	563	0.94	1.05	1.05
E-SBA-15	360	0.57	2.60	1.30
P-SBA-15	236	0.41	3.50	1.16
A-SBA-15(OP)	552	0.59	1.10	1.10
E-SBA-15(OP)	430	0.62	2.76	1.38
P-SBA-15(OP)	416	0.46	2.78	0.93

[a] Determined by elemental analysis. [b] Obtained by dividing the nitrogen concentration by the number of N atoms in the single silane chain.

branch of the isotherms on the silica surface (Fig. 2). The bare silica SBA-15 sample is characterized by two families of pores, the first one with a maximum centered at *ca.* 85 Å and the second with dimensions from 20 to 40 Å, which has been assigned to the pores connecting the bigger mesopores (Fig. 2A).[41] After the post-synthesis functionalization, for the A-SBA-15 sample, the pore at *ca.* 85 Å shifts at *ca.* 80 Å and a family of smaller pores located from 20 to 40 Å disappears, when a new family of pores with a dimension of 40–60 Å appears. E-SBA-15 and P-SBA-15 samples show the same behavior, even if pores with dimensions of 40–60 Å are less numerous and the principal pores are shifted at 80 and 70 Å, respectively. The total pore volume for SBA-15 was 0.98 cc per g whereas for A-SBA-15, E-SBA-15 and P-SBA-15 samples they were 0.94, 0.57 and 0.41 cc per g, respectively. The A-SBA-15(OP) sample is characterized by two families of pores at *ca.* 35 and 50 Å, definitively smaller than the analogous A-SBA-15 grafted sample, whereas a larger pore distribution was found for the other two samples prepared using a one-pot method. In particular, the E-SBA-15(OP) sample has pores in the 30–90 Å range with two maxima at 50 and 70 Å. Finally, the P-SBA-15(OP) material showed the broadest pore distribution and disordered pores with dimensions between 30 and 110 Å (Fig. 2B). It can be noticed that increasing the silane length, the volume of pores centered at 50 Å decreases progressively in favor of more disordered pore structures, in good agreement with XRD and TEM analysis. The pore volume of one-pot prepared samples is reported in Table 1.

The concentration of nitrogen atoms introduced in the samples by different preparation procedures is reported in Table 1. It was estimated that the N content (expressed as mmol of N per g of sample) is *ca.* 1.05, 2.60 and 3.50 mmol g^{-1} for the grafted A-SBA-15, E-SBA-15 and P-SBA-15 samples, respectively. The concentration of silane molecules on the grafted A-SBA-15, E-SBA-15 and P-SBA-15 samples was also calculated by dividing the total amine loading by 1, 2, and 3, respectively (*i.e.* by the number of nitrogen atoms in each silane chain). All these data are summarized in Table 1. It is evident that the silane concentration is similar for all samples, as also expected from the fact that the same molar concentration of organic species was used for the grafting procedure. This also suggests that steric hindrance problems between the organosilane chains are not significant during post-synthesis grafting.

The TGA analysis of the parent SBA-15 sample allowed the estimation of the concentration of the surface silanol species by using eqn (1), where %OH = TGA weight loss between 200 °C and 1100 °C, due to the condensation of silanols group, 2 is the number of SiOH needed to form a water molecule by condensation, N_A = Avogadro number (6.022×10^{23}), $M.W._{H_2O}$ = molecular weight of water (18.01 g mol^{-1}) and S.S.A. is the Specific Surface Area of the parent sample, estimated by N_2 physisorption analysis.

$$\mathrm{SiOH}\ (\mathrm{nm}^{-2}) = \frac{\%\mathrm{OH}}{100 - \%\mathrm{OH}} \times \frac{2 \times N_A}{M.W._{H_2O} \times S.S.A} \quad (1)$$

The concentration of surface silanols calculated using eqn (1) is *ca.* 5.1 SiOH nm^{-2}.

After the grafting procedure, assuming a complete reaction between the silane and the hydroxyl groups of the surface, *ca.* 3 SiOH nm^{-2} are condensed for all samples during the aminosilane grafting and tridentate complexes are formed. This is an overestimation in that bidentate complexes may also be produced during the grafting procedure. Concerning one-pot prepared samples, the concentration of N species is similar to the grafted materials for all the samples.

The presence of organic species grafted on the SBA-15 surface silica was evaluated by FT-IR spectroscopy (Fig. 3).

In the high frequency range, the FT-IR spectrum of the pure SBA-15 silica sample (Fig. 3A) is characterized by the presence of two main bands located at 3745 cm^{-1} (sharp) and at *ca.* 3500 cm^{-1} (broad). The band at 3745 cm^{-1} is due to the stretching mode of the isolated silanol groups,[42] whereas the broad absorption band at 3500 cm^{-1} is due to the stretching mode of OH species interacting with each other through H-bonding.[21]

As expected, after the grafting procedure the bands due to surface SiOH species appear to be strongly decreased in intensity (this is especially evident for E-SBA-15 and P-SBA-15 samples in which this band has an exceedingly low intensity) due to the fact that SiOH species are involved in the grafting procedure. Interestingly, a residual amount of isolated SiOH species is still present on the A-SBA-15 sample (Fig. 3A). Moreover, a broad band in the 3600–2500 cm^{-1} range is visible in the IR spectrum of the grafted samples. This band can be related to the formation

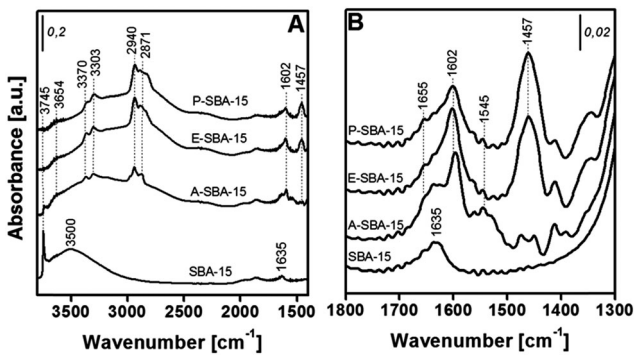

Fig. 3 Frame A: FT-IR spectra of bare SBA-15 and grafted samples. Frame B: enlargement of the FT-IR spectra in the 1800–1300 cm^{-1} range. Spectra were recorded outgassing the samples at r.t. for 30 minutes.

of H-bonding interactions between surface silanols and amino groups of silane species grafted on the surface.

The IR spectra of the grafted samples are characterized by the presence of complex absorption in the 3500–2500 cm^{-1} range, in which different components at 3370, 3303, 2940 and 2871 cm^{-1} are visible. The absorption bands at 3370 and 3303 cm^{-1} are assigned to the asymmetric and symmetric stretching modes of NH_2 groups, respectively, whereas the bands at 2940 and 2875 cm^{-1} are assigned to the asymmetric and symmetric stretching modes of CH_2 moieties of the silane groups grafted onto the silica surface by the grafting procedure. The absorption bands in the low frequency region (Fig. 3B) are assigned to the scissoring mode of NH_2 groups (band at 1600 cm^{-1}) and to the bending modes of CH_2 groups (band located at 1457 cm^{-1}).[21] It can be noted that for the A-SBA-15 sample, a fraction of NH_3^+ species is also present, as attested by the bands at 1655 and 1545 cm^{-1}.[21] The presence of the organic groups grafted on the SBA-15 silica surface was confirmed by the T^3 ($Si(OSi)_3C$) and T^2 ($Si(OSi)_2(OCH_3)C$) signals in ^{29}Si MAS NMR spectra, and by well-defined resonances of carbon atoms of the organic chains in the ^{13}C CPMAS NMR spectra (see Fig. S3 and S4 in the ESI†).

Similar IR absorption bands were also found for SBA-15 related samples prepared by a one-pot procedure (Fig. S5 in the ESI†). For these samples, it is interesting to note that the one-pot synthesis procedure, which is carried out at low pH, induces the protonation of the amino groups grafted on the sample surface, especially for A-SBA-15(OP) and E-SBA-15(OP) samples (as evidenced by FTIR analysis, Fig. S5 in the ESI†). This is probably the main reason why these samples are less reactive towards CO_2 with respect to post-synthesis grafted materials (*vide infra*). In the following part, in order to have additional insight into the role of the surface species in the CO_2 capture process, only the data related to the more reactive grafted samples will be reported.

To account for all the protonic species in the grafted systems, single pulse excitation ^1H MAS NMR experiments were performed (Fig. 4). The direct acquisition of spectra allows the observation of both mobile and rigid components quantitatively as the line widths reflect and distinguish their presence. The pristine samples A-SBA-15 and P-SBA-15 show sharper narrow resonances at around 0.7 ppm due to methylene protons close to Si atoms. All the remaining methylene protons appear as a sharp peak at around 1.2 ppm. In addition, a peak at around 2 ppm due to surface silanols was also visible. On the contrary, no sharp resonances were detected for the sample E-SBA-15. Here, all the EAPTS chains are in a confined environment where they experience reduced mobility. This is probably due to the inter- and/or intra-molecular interactions they are involved in. The former type of interaction is feasible with the silica surfaces at the interface through the involvement of non-covalent bindings by silanols and water, which is probably remaining after the thermal treatment performed before the analysis. Such a possibility will lead the EAPTS side chains to adopt several conformations and result in heterogeneous broadening of resonance lines. However, very fast motions of the side chains in A-SBA-15 and P-SBA-15 average out all ^1H–^1H dipolar interactions leading to narrow resonances. On the other hand, a very broad resonance peak centered at 5.7 ppm is visible in all the spectra and is associated with non-covalently interacting NH_2 groups, with physisorbed water remaining after the thermal activation treatment and hydrogen bonded silanols.

The rotor synchronized Hahn-echo sequence was also applied to record the ^1H NMR spectra with a τ delay time of 6700 μs (Fig. 4). The delay time was chosen as an optimized compromise between the signal decay owing to relaxation and the resolution gain owing to longer delay times. Using the rotor synchronized Hahn-echo sequence with long delay time results in the selective detection of mobile species. For this experiment, we rely on the differences in spin–spin relaxation of aliphatic chains, which are either mobile or rigid depending on their interactions with the silica surface. Differentiation between rigid and mobile components can be accomplished in terms of the observed width of the resonance peaks. While the mobile components are detected as sharp narrow peaks, broader lines due to rigid components often are not resolved from the baseline.

Fig. 4 shows the ^1H NMR spectra recorded using the Hahn-echo sequence of the samples before $^{13}CO_2$ adsorption. The A-SBA-15 and P-SBA-15 samples show sharper narrow resonances due to methylene protons of organic side chains. In addition, a peak at around 2 ppm was also visible which was due to the isolated surface silanols. On the contrary, no sharp resonances were detected for the sample E-SBA-15 and are associated with spatial confinement of EAPTS chains. This spectrum confirms that inter- and/or intra-molecular interactions in pristine E-SBA-15 occur in/among the organic chains. One small peak at 6.9 ppm was also visible in all samples and was due to protonated amino groups. The ^1H NMR experiments confirm that the EAPTS chains grafted on the SBA-15 surface experience reduced mobility compared to other samples. The possibility of molecular interactions among the grafted chains can be estimated by comparing the average free space around each amino-silane with a reasonable approximation of the molecular length. In Table 2, we report the average area of each silane domain on the surface (as the inverse of the organosilane density), and thus the average

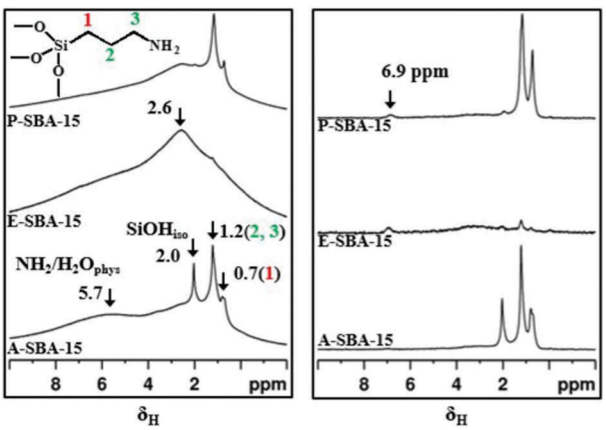

Fig. 4 ^1H MAS NMR (left panel) and Hahn-echo NMR spectra (right panel) of hybrid SBA-15 samples prepared by the grafting procedure.

Table 2 Distances between alkyl chain of silane in A-SBA-15, E-SBA-15 and P-SBA-15 silica samples

Sample	Silane density [no. of chains per nm^2]	Intermolecular distance [Å]	Length of silane[a] [Å]
A-SBA-15	0.9	10.5	5.3
E-SBA-15	1.1	9.5	7.1
P-SBA-15	1.0	10.0	8.9

[a] Length of the organosilane as determined by the geometry optimization described below.

intermolecular distance (as the square root of this area); the chain lengths were obtained from the *ab initio* geometry optimizations described below.

The comparison shows that interactions are quite unlikely between APTS chains, whereas they could be observed between EAPTS and PAPTS. It has to be noted that these observations are only qualitative because they suppose a homogeneous distribution of organic chains.

The structure of the amino-silanes grafted on the silica surface was simulated theoretically using the method and the model clusters described above. First, one molecule of each organosilane (APTS, EAPTS and PAPTS) was added to cluster I, and the three adduct geometries were optimized. The final structures are shown in Fig. 5: in the APTS-I model the relatively short chain and the rigidity of the tridentate organic–silica bond prevent the amino group to bend towards the surface, whereas the other, longer chains can lie down on the silica surface. One or two H-bonds were formed between silanols and amino groups in EAPTS-I and PAPTS-I, respectively: in the former case the bond appears to be stronger (O–N distance 2.5 Å in EAPST-I, 2.7 and 2.8 Å in PAPTS-I); dispersion forces also provide a large contribution to the interaction energy between organic chains and the surface (the weight of H-bond and dispersion

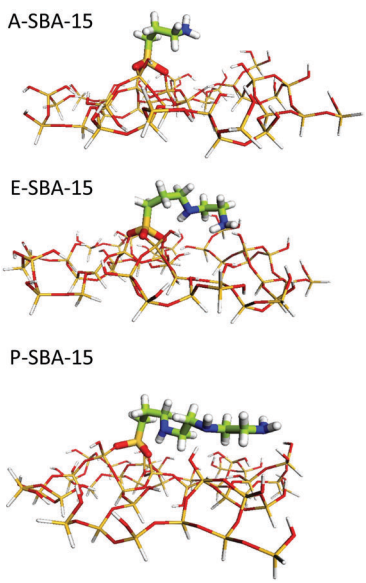

Fig. 5 Optimized structures of the adducts of APTS, EAPTS and PAPTS on silica model cluster I.

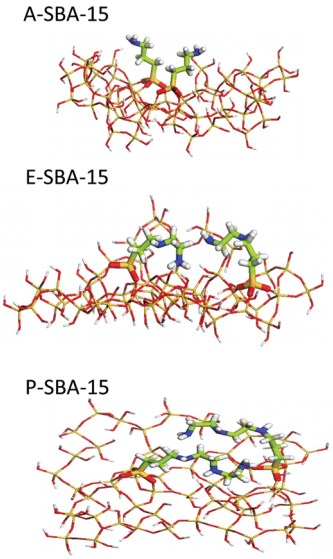

Fig. 6 Optimized structures of the adducts with two molecules of APTS, EAPTS and PAPTS on silica model cluster II.

interactions are similar, though the separation between them is somehow arbitrary).

To gain some insight into intermolecular interactions also, we optimized the structure of adducts with two molecules grafted on the larger cluster II, with the results reported in Fig. 6. The behavior of all the organosilane chains is similar to that observed for the smaller cluster: APTS tends to remain "perpendicular" to the surface, whereas both EAPTS and PAPTS lie closer to the silica surface. However, not all the PAPTS nitrogen atoms are H-bonded to the surface, since there are not enough silanol groups in a suitable position: this suggests that PAPTS motions could be less hindered, even if this is just one of the possible conformations of the hybrid system.

Note that the data in Tables 1 and 2 imply a density of grafted amino-silane of 0.9–1.1 molecules per nm^2 for all the systems: since the surface of the clusters, as said above, is around 2.5 and 4 nm^2, respectively, the simulated densities with one molecule on cluster I and two on cluster II appear to be underestimated to some extent. Then two more adducts were optimized, grafting on cluster II three EAPTS or PAPTS molecules, respectively, since steric effects are expected to be more relevant for these systems than for the shorter APTS chains. In fact, as shown in Fig. 7, in both structures the third organosilane molecule is not able to approach the silica surface, and it remains almost perpendicular to the surface.

Note that in these models a homogeneous distribution of EAPTS and PAPTS on the surface was assumed, leading to distances between the organic chains of about 12 Å in the adducts with two molecules, and about 9 Å with three molecules. Some caution is required to interpret this result, since the use of a finite cluster model could be altered by border effects (in other words, the effective surface area could be smaller than 4 nm^2, as obtained by the cluster side dimensions): nonetheless, these optimized adducts suggest that some organosilane chains, when the density is around 1 molecule per nm^2, can be quite free to move far from the silica surface.

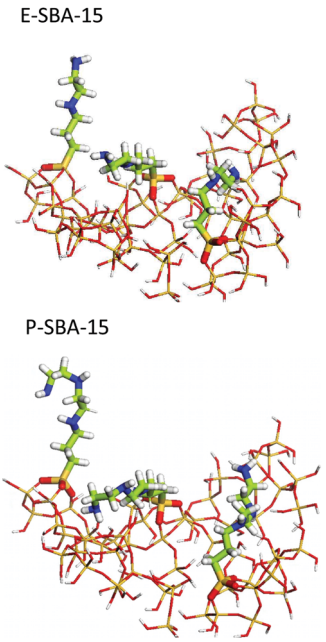

Fig. 7 Optimized geometry of the adducts with three EAPTS and three PAPTS molecules on silica cluster II.

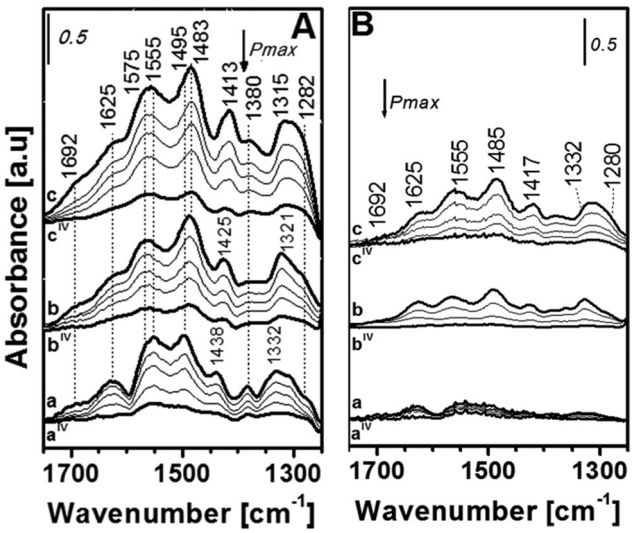

Fig. 8 FTIR spectra, in the 1750–1250 cm^{-1} region, of CO_2 adsorbed (P_{max} = 60 mbar) at BT on the grafted samples (frame A): A-SBA-15 (curves a-a^{IV}), E-SBA-15 (curves b-b^{IV}) and P-SBA-15 (curves c-c^{IV}), and samples prepared using a one-pot method (frame B): A-SBA-15(OP) (curves a-a^{IV}), E-SBA-15(OP) (curves b-b^{IV}) and P-SBA-15(OP) (curves c-c^{IV}). The arrows indicate decreasing CO_2 pressure. Spectra are reported after subtraction of the spectrum of the bare sample (before CO_2 interaction) used as a background.

Study of reactivity between CO_2 and organo-modified SBA-15

Both infrared spectroscopy and solid-state NMR of the adsorbed carbon dioxide were used to study the interactions between CO_2 and the basic group of the functionalized silica samples.

The IR spectra collected after admission of 60 mbar of CO_2 at beam temperature (BT) on the samples prepared by both post-synthesis grafting and a one-pot procedure are reported in Fig. 8.

For the A-SBA-15 sample (Fig. 8, curve a), the admission of CO_2 leads to the formation of carbamate species as testified by bands located at 1555, 1495 and 1438 cm^{-1} (see Table 3 for the assignment of the main bands). Moreover, peaks due to the presence of carbamic acid can also be found at 1692 and 1380 cm^{-1}.[43] By decreasing progressively CO_2 pressure (Fig. 8, curves a^{I}–a^{IV}) bands related to carbamates and carbamic acid species progressively decrease in intensity thus indicating that part of the formed species is removed by the outgassing procedure. From deconvolution of bands between 1410 and 1440 cm^{-1}, chosen as a representative of carbamate formation, and of the band at 1380 cm^{-1}, a representative of carbamic acid (data not shown for the sake of brevity), it has been observed that the intensity of the bands decrease in the same way both for carbamate and carbamic acid bands, thus indicating that the two species have approximately the same stability. Nevertheless, these species are in strong interaction with the sample surface, as witnessed by the fact that IR bands do not completely disappear upon outgassing at BT for 30 min (Fig. 8, curve a^{IV}).

Concerning the E-SBA-15 and P-SBA-15 samples (Fig. 8, curves b-b^{IV} and c-c^{IV}), the admission of CO_2 also leads to the formation of carbamic acid and carbamate species. The deconvolution and integration of IR curves allowed us to estimate the ratio between the carbamates and carbamic acid formed upon CO_2 adsorption on the different samples. It was derived that the amount of carbamates is similar for all samples whereas the quantity of carbamic acid increases passing from the A-SBA-15 to P-SBA-15 sample.

In addition, the presence of a shoulder located at *ca.* 1575 cm^{-1} in E-SBA-15 and P-SBA-15 samples is due to the deformation of NH_2^+ or due to the combination of N–H deformation and C–N stretch vibrations in carbamates. This indicated that the samples containing more than one amino group in the chain react with CO_2 to form an intramolecular carbamate ammonium salt.[44] The occurrence of intermolecular species is also indicated by the modification of the asymmetric bending of NH_3^+ (1625 cm^{-1}): the signal is almost resolved for the A-SBA-15 sample, whereas the absorption band becomes broader in the case of the E-SBA-15 and P-SBA-15 samples and this suggests the presence of residual NH_2^+ groups.

Finally, shifts at a lower frequency of both the symmetric stretching of the COO^- group (from 1438 cm^{-1} to 1413 cm^{-1}) and the $NCOO^-$ skeletal vibration (from 1332 cm^{-1} to 1315 cm^{-1}), probably due to the increase of the length of organic chains, were observed.

As a matter of fact, in grafted samples the intensity of IR absorption increases along with the concentration of N atoms (*i.e.* on passing from the A-SBA-15 to the P-SBA-15 sample), thus suggesting that the higher the concentration of amine groups, the higher the reactivity towards CO_2.[15]

A similar behavior was observed for the samples prepared by a one-pot procedure. In this specific case, however, although the detected IR bands are in similar positions to those observed for grafted samples (thus suggesting the formation of the same

Table 3 Assignments of the main FTIR bands formed upon CO_2 adsorption on functionalized SBA-15 samples

Wavenumber [cm^{-1}]	Assignment	Ref.
1692	Stretching (C═O) of carbamic acid	45 and 46
1625	Asymmetric bending of NH_2^+/NH_3^+	45, 47–50
1575	Deformation of NH_2^+ or combination of N–H deformation and C–N stretch vibrations in intermolecular carbamates	44
1555	Asymmetric stretching of C═O group of carbamate	50
1495–1483	Stretching of $NHCOO^-$ of carbamate	45, 46, 48–53
1500–1485	Symmetric bending of NH_2^+/NH_3^+	45, 47–51
1438–1413	Symmetric stretching of COO^- group of carbamate	45, 47 and 52
1380	Bending of OH in carbamic acid	43 and 52
1332–1315	$NCOO^-$ skeletal vibration	47
1282	Rocking of NH_3^+	45

species upon contact with CO_2), the intensity of absorption bands appeared to be significantly lower compared to the analogous post-synthesis grafted samples. Although the two series of samples have a similar amount of N species (except the one-pot prepared samples with APTS species that has higher N content with respect to the grafted analogous sample), the low reactivity associated with the samples prepared *via* a one-pot method can be explained considering that this procedure led to the formation of protonated amino groups, not suitable for reaction with CO_2.

The IR assignments of the relevant peaks in the range are listed in Table 3.

Detailed information on the changes of the surface structures and the dynamics of the organic-functionalized SBA-15 samples prepared by post-synthesis after the introduction of $^{13}CO_2$ was obtained by means of ^{13}C CPMAS NMR. With respect to the pristine samples, no dramatic changes in the chemical shifts of aliphatic carbons were observed for $^{13}CO_2$ chemisorbed samples; however, broadening of all resonances are evident (Fig. 9). Moreover, an additional resonance peak at 164 ppm was clearly visible in all the samples and was attributed to the presence of carbamate groups.[54] Moore *et al.* has studied CO_2 adsorption on hyperbranched amine polymers grown from the mesoporous silica SBA-15 which exhibited a mixture of chemisorption products, including carbamate, carbamic acid and bicarbonate moieties.[55] The resonance peak at 164 ppm lies near the chemical shift values expected for typical carbamic acid (160 ppm), bicarbonate (163 ppm) and carbamate (164 ppm) species. The full width at half-maximum (fwhm), around 4 ppm, of this resonance is larger than the chemical shift difference (~3 ppm) between these products. Therefore, the presence of carbamic acid and bicarbonate moieties cannot be excluded from the systems studied here. On the other hand, Moore *et al.* observed the mixture of chemisorption products due to the presence of primary, secondary, and tertiary amines, which enables multiple reactions through multiple pathways. Furthermore, they have observed that upon evacuation more loosely bound chemisorbed CO_2 products were desorbed. In our study mostly firmly bound carbamate species are found on the surface of organically modified SBA-15, probably because of the absence of tertiary amines.

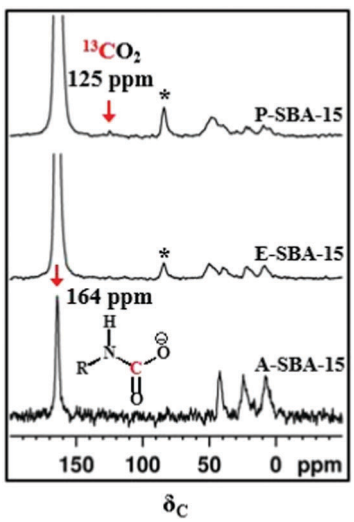

Fig. 9 ^{13}C CPMAS NMR spectra of $^{13}CO_2$ adsorbed on grafted SBA-15 samples. A cross polarization contact time of 2 ms and a MAS rate of 10 kHz were used in all the experiments. * Denote spinning side-bands.

Furthermore, ^{13}C CPMAS NMR data revealed the presence of an additional fraction of physisorbed $^{13}CO_2$, especially in the case of P-SBA-15. Previous studies have demonstrated the formation of a carbamate group as well as the physisorption of $^{13}CO_2$ in amine-modified porous materials.[50] The intensity of the signal due to the carbamate species increases along with the concentration of N atoms. These results, in line with those obtained by FTIR, suggested that the amount of amino groups influence the reactivity with $^{13}CO_2$.

Fig. 10 shows the ^1H MAS NMR and Hahn-echo NMR spectra of the samples after $^{13}CO_2$ adsorption. A reduction in mobile components was clearly visible in the sample P-SBA-15 after the $^{13}CO_2$ adsorption. However, the peak due to surface silanols was missing from the sample A-SBA-15 after $^{13}CO_2$ adsorption although the behavior of side chains was similar to that before the adsorption. An increase in the amount of protonated amino groups was clearly visible in all the three samples. Before the introduction of $^{13}CO_2$, the A-SBA-15 and P-SBA-15 samples showed a similar amount of mobile and rigid components. On the contrary, only rigid components were visible in the sample E-SBA-15 as confirmed by the absence of sharp peaks in the high resolution Hahn-echo NMR spectra presented here. However, an increase in the rigid part was clearly observed for all the samples after their exposure to $^{13}CO_2$. In conclusion, the behavior

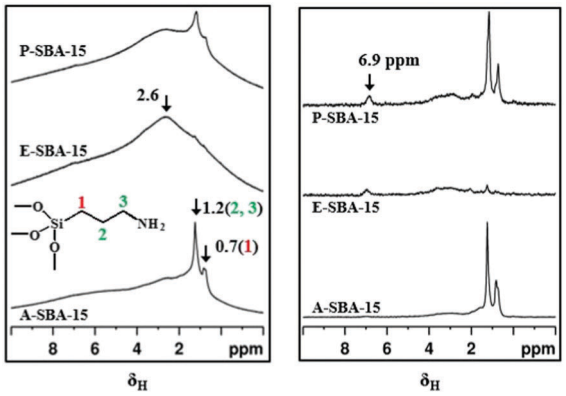

Fig. 10 ^{1}H MAS NMR and Hahn-echo NMR spectra of samples after $^{13}CO_2$ adsorption on SBA-15 grafted samples.

of different chains at the interface is diverse as they are capable of non-covalent interactions. Such interactions will lead to a distribution of chain conformations at the interface, which are reflected as broad resonance lines. Nevertheless, a significant fraction of these chains in samples A-SBA-15 and P-SBA-15 is capable of isotropic motions, which are revealed as sharp peaks. The conversion of amino group into carbamate species upon $^{13}CO_2$ introduction does not influence the molecular dynamics of side chains at the interface.

Study of the CO_2 capture capacity

The isotherms relative to the adsorption at 30 °C of carbon dioxide on the three amino-functionalized SBA-15 samples are reported, as a function of the CO_2 equilibrium pressure (see full symbol curves) in Fig. 11 and Fig. S6 (ESI†) (these latter isotherms were calculated at very low equilibrium pressures). The CO_2 uptake capacity of the three samples, at pressures lower than 150 mbar, follows the trend reported in the FT-IR adsorption experiments, *i.e.* P-SBA-15 > E-SBA-15 > A-SBA-15. Independently from the sample, the three quantitative isotherms indicate a specific adsorption pathway in which it is possible to distinguish the initial adsorption of carbon dioxide on the more reactive amine sites at low pressures (with the formation of carbamate species),[56,57] followed by filling of the available pore volume at higher pressure. In particular, both systems grafted with alkylamine chains containing more than one amino group (E-SBA-15 and P-SBA-15) exhibit isotherms with a steep increase (more evident for the P-SBA-15 sample) for pressure lower than 10 mbar and a gradual increase from 5 to 500 mbar. Still, the quantitative isotherms of the systems containing two or three amino groups change behaviour at higher CO_2 pressures. For p > 300 mbar, in fact, the E-SBA-15 isotherm is still clearly growing with respect to the P-SBA-15 isotherm that is slowly approaching its plateau. The material functionalized with the plain amino-propyl group (A-SBA-15) exhibits a peculiar isotherm with an evident step between 60 and 100 mbar and an appreciably lower overall adsorption capacity per gram of sample, especially at low equilibrium pressures. The definitely lower amount of adsorbed CO_2 in the case of A-SBA-15 is related to the different adsorption method of this molecule in the presence

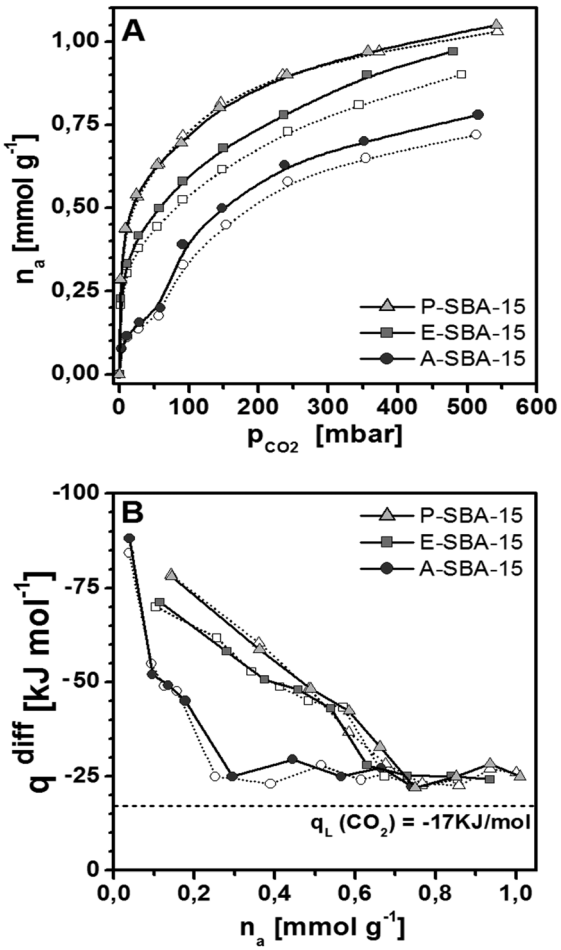

Fig. 11 Frame (A) quantitative isotherms related to the adsorption at 30 °C of CO_2 on A-SBA-15 (circle), E-SBA-15 (squares) and P-SBA-15 (triangle) samples. Frame (B) differential molar adsorption heats related to the adsorption of CO_2 on the grafted SBA-15 samples. The dashed horizontal line represents the standard molar enthalpy of liquefaction of CO_2 at 298 K. Solid symbols represent the primary adsorption runs and empty symbols the secondary adsorption ones.

of a shorter alkylamine chain. In this case, in fact, the formation followed by stabilization of the carbamate species occurs between two adjacent amine chains (intermolecular CO_2 adsorption): only the amino groups located at the right distance are effective adsorption sites for carbon dioxide.[56] This problem is exceeded in E-SBA-15 and P-SBA-15 in which the adsorption of carbon dioxide proceeds *via* the formation of intramolecular carbamate species.[57] In this last case all the alkylamine chains are potentially able to react with one CO_2 molecule forming and stabilizing alkylammonium carbamate. The intramolecular cooperative adsorption with the formation of alkylammonium carbamate occurs between the NH_2 and the NH moieties of the alkylamine chain. For this reason, even if the P-SBA-15 sample contains two NH groups the capture of a second CO_2 molecule is not possible and, therefore, the overall CO_2 adsorption capacity is only slightly higher in the case of P-SBA-15. On the contrary, as mentioned above, at low pressure, P-SBA-15 is able to adsorb a definitely higher amount of carbon dioxide. These data suggest that,

probably, the intramolecular species are more efficiently formed by two amines separated by more than two atoms, *i.e.* when the amine chain is more flexible *(vide supra* the computational part).

Moreover, the presence of the step in the isotherm of the A-SBA-15 sample can be probably derived from the possibility of this material to interact with CO_2 in two different ways: (i) through the cooperation of an amine chain with a surface residual silanol group (as demonstrated by the FT-IR analysis, the residual amount of the isolated SiOH species is clearly higher in the case of A-SBA-15) forming a carbamic acid species stabilized by the interaction with a surface OH group: (ii) through the formation of a carbamate species between two adjacent amine chains. The intermolecular amine–amine adsorption is probably favoured at higher equilibrium pressures. This phenomenon could explain the presence of the step at around 60 mbar.

Also E-SBA-15 and P-SBA-15 can interact with CO_2 in two different ways: (i) through the cooperation of an amine chain with a surface residual silanol group with the formation of carbamic acid or (ii) through the formation of an intramolecular carbamate species. However, their CO_2 adsorption isotherms do not exhibit the step at low equilibrium pressures (as A-SBA-15), probably because these two interaction ways are both favoured independently from the CO_2 pressure.

Moreover, taking into account that from IR data it was derived that the quantity of carbamic acid species increases on passing from the A-SBA-15 to P-SBA-15 sample, it is clear that, despite the lower amount of the residual isolated SiOH species of E-SBA-15 and P-SBA-15 with respect to A-SBA-15, the simultaneous interaction of CO_2 with an amine and a residual surface OH group (with the formation of carbamic acid) seems to be favoured due to the higher mobility of longer amine chains that allows their approach also to far OH species during the cooperative interaction with CO_2. In particular, the higher the length of the grafted alkylamine chain, the higher the amount of carbamic acid formed.

Comparing our results to those reported by Yoo *et al.*[15] for similar sorbents (*i.e.* SBA-15 grafted with APTS, EAPTS and PAPTS), but containing a lower amount of organosilane, we can see a significant effect of the silane density. In the work cited, in which the silane concentration is deliberately low (0.45 mmol g^{-1}), the CO_2 adsorption capacity values are 0.05, 0.08 and 0.125 mmol g^{-1}, respectively, for A-SBA-15, E-SBA-15 and P- SBA-15 at a pressure of 60 mbar. However, in our study, in which the silane concentration is around 1 mmol g^{-1} (that is around the double that in the cited work), the CO_2 adsorption capacity values at the same pressure are significantly increased for each sample: 0.20, 0.50 and 0.64 mmol g^{-1}, respectively, for A-SBA-15, E -SBA-15 and P-SBA-15 (*i.e.* more than four times of the values reported by Yoo). These values suggested that the high amine loading on the SBA-15 surface is effective to increase the adsorption capability towards CO_2 probably because of the propinquity of reactive species on the surface. The fact that this effect is more pronounced for E-SBA-15 and P-SBA-15 samples could be related to a favourable arrangement of organic chains on the silica surface at high silane loading.

The comparison between primary (full symbols) and secondary (empty symbols) adsorption isotherms in Fig. 11(A) highlights an almost total reversibility of the adsorbed CO_2 in the case of A-SBA-15 and E-SBA-15, and a total reversibility in the case of P-SBA-15. These last results are not in perfect agreement with the data reported in the FT-IR section probably in relation to the short outgassing time employed upon FTIR CO_2 adsorption with respect to the calorimetric analysis. Differential molar adsorption heats of the various samples are reported in Fig. 11(B) and Fig. S6(B) (ESI†) (for very low coverages) as a function of the adsorbed amounts. These values are in agreement with the data reported in the literature for similar systems.[58,59] For what concerns the A-SBA-15 material, the adsorption enthalpy starts at very high values (higher than -90 KJ mol^{-1}; zero-coverage differential heat of adsorption $q_o \sim -120$ KJ mol^{-1}) and this suggests the presence of a small fraction of extremely energetic sites, *i.e.* the strongest in terms of energy of interaction and, therefore, active in the earliest stages of the adsorption process (in this specific case, they are probably, couples of amine chains with a particularly favourable position for the formation of the intermolecular carbamate species). Then, the adsorption heat decreases fast with increasing carbon dioxide loading to about -25 KJ mol^{-1}. The enthalpy values in the -90 to -45 KJ mol^{-1} range can be attributed to the strong interaction between the carbon dioxide molecules, the adjacent amine groups and the residual surface silanols forming intermolecular carbamate species and carbamic acid species. Then, once all available amine and SiOH groups (*i.e.* located at the right distance for the effective cooperative adsorption of CO_2) have interacted with CO_2, the gas adsorbs on less reactive surface sites (residual surface silanols). A very similar trend can be observed for the other two samples (E-SBA-15 and P-SBA-15). In this case, however, the initial adsorption enthalpy starts at lower values (around -80 KJ mol^{-1}; zero-coverage differential heat of adsorption $q_o \sim -100$ KJ mol^{-1}) and proceeds declining slowly to ~ -45 KJ mol^{-1}. The definitely lower values of enthalpy at zero-coverage, observed for these two samples with respect to A-SBA-15, can be explained considering that, as demonstrated by the computational calculations, the longer amine chains (EAPTS and PAPTS) can lie down on the silica surface and form H-bonds with the residual surface silanols. Before the interaction with the CO_2 molecules, these H-bonds have to be broken leading to a decrease of the first values of adsorption heat for these samples. The enthalpy values in the -80 to -50 KJ mol^{-1} range can be associated with the CO_2 adsorbed *via* intramolecular interactions.[57,58] Then, when all the amine groups have interacted with CO_2 the adsorption enthalpy decreases up to -25 KJ mol^{-1}, tending to the asymptotic value of carbon dioxide molar liquefaction enthalpy (-17 KJ mol^{-1}) which is characteristic of the uptake phase dominated by metastable liquid-like physical adsorption.

The chemisorbed CO_2 amount can be easily derived from Fig. 11(B), considering the amount of adsorbed CO_2 corresponding to the enthalpy values (in the range between -90 and -40 KJ mol^{-1}) associated with the CO_2 adsorption *via* intermolecular or intramolecular interactions with the alkylamine

chains, thus avoiding the contribution of physisorbed CO_2. The chemisorbed amount on A-SBA-15, E-SBA-15 and P-SBA-15 is *ca.* 0.2, 0.6 and 0.7 mmol g^{-1} respectively, apparently much lower with respect to the amino group content (*ca.* 1, 2.6 and 3.5 mmol g^{-1} for A-SBA-15, E-SBA-15 and P-SBA-15, respectively). For what concerns the A-SBA-15 sample, the formation followed by stabilization of the carbamate species occurs between two adjacent amine chains and only two amino groups located at the right distance are effective adsorption sites for carbon dioxide. This type of interaction is responsible for the low CO_2 chemisorbed amount ($\sim$0.2 mmol g^{-1}) of this material with respect to its content of amino groups (1 mmol g^{-1}). In fact, two different amino groups are necessary to form the carbamate species and, therefore, the amount of CO_2 that could be actually chemisorbed by this material is no higher than 0.5 mmol g^{-1} and, moreover, the number of amine chains located at the right distance to allow the formation of the carbamate species can be restricted. On the other hand, in the case of E-SBA-15 and P-SBA-15 the adsorption of carbon dioxide proceeds *via* the formation of intramolecular carbamate species. Potentially, all the alkylamine chains can interact with one CO_2 molecule by means of a NH_2 group and a NH moiety at the same time: in the case of E-SBA-15, containing $\sim$2.6 mmol g^{-1} of amino groups, the potential chemisorbed CO_2 uptake cannot be higher than $\sim$1.3 mmol g^{-1}, whereas for P-SBA-15 (with an amino groups content of $\sim$3.5 mmol g^{-1} and containing one NH_2 group and two NH moieties for each chain) one third of the amino groups does not take part in the intramolecular cooperative adsorption and, as a consequence, the potential amount of CO_2 that can be adsorbed by the amine chains is not higher than $\sim$1.2 mmol g^{-1}. However, for E-SBA-15 and P-SBA-15 the actual chemisorbed CO_2 uptake is $\sim$0.6 and $\sim$0.7 mmol g^{-1} respectively *i.e.* definitely lower than 1.3 and 1.2 mmol g^{-1}. As demonstrated by the computational calculations, the longer amine chains (EAPTS and PAPTS) lie down on the silica surface and form H-bonds with the residual surface silanols that have to be broken before the interaction with the CO_2 molecules. Probably, this circumstance may not always occur, thereby explaining the lower amount of chemisorbed CO_2 compared to the real amino groups of these two materials.

Study of CO_2 capture capacity under post-combustion conditions

The adsorption of CO_2 was also monitored using the ZLC method to determine quantitatively the CO_2 uptake. This is an innovative and advantageous screening method for amino-grafted silica adsorbents, because it requires a very small amount of samples (10–15 mg) and short experimental time (about 1 hour per test).

Fig. 12A shows an example of the ZLC desorption curve for the P-SBA-15 sample. The data are plotted as dimensionless concentration, C/C_0 (C_0 = CO_2 concentration in the gas phase at equilibrium), *vs.* the volume of gas eluted Ft (F = inlet flowrate of the carrier, He). The plot includes the blank curves, *i.e.* the response of the system when no sample is loaded. Based on the mass balance of the column the difference between the area under the desorption curve of the sample and the blank is proportional to the amount adsorbed: the CO_2 uptake can then be calculated by integration.[23,60]

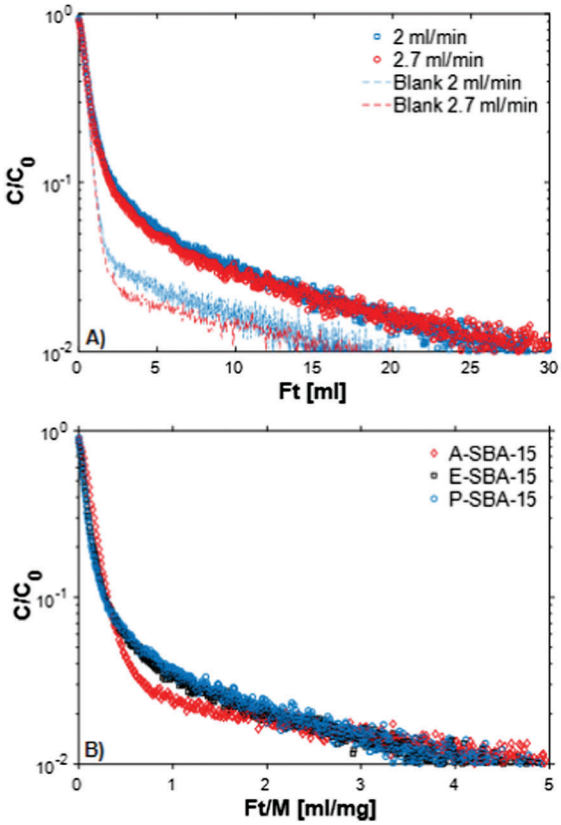

Fig. 12 Section (A) – ZLC desorption curves for P-SBA-15 sample and blank curves at 2 and 2.7 mL min^{-1} flow rates. Section (B) – ZLC desorption curves for A-SBA-15, E-SBA-15 and P-SBA-15 samples (CO_2 partial pressure: 0.1 bar, flow rate: 2 mL min^{-1}, T: 35 °C).

By normalizing the Ft plot by the mass of the sample, M, the ranking of the CO_2 uptake for each SBA-15 sample can be visually compared, as shown in Fig. 12B. Table 4 summaries the capacities calculated for the ZLC desorption curves for the different samples (note that the ZLC experiments were carried out at 0.1 bar partial pressure of CO_2 and 35 °C). The sequence of the CO_2 capacities is in excellent agreement with the volumetric measurements (Fig. 11), with P-SBA-15 > E-SBA-15 > A-SBA-15.

It is worth noting that the ZLC method measures the amount desorbed from the sample. For a purely physisorption process

Table 4 Comparison between ZLC and calorimetric results for CO_2 adsorption at low pressure

	ZLC[a]			Calorimetric measurements[b]
Sample	CO_2 [mmol g^{-1}]	CO_2 [mg g^{-1}]	CO_2/N ratio	CO_2 [mmol g^{-1}]
SBA-15	0.16	6.2	—	—
A-SBA-15	0.23	9.2	0.20	0.31
E-SBA-15	0.39	16.7	0.15	0.51
P-SBA-15	0.51	22.4	0.15	0.68

[a] ZLC working conditions: (i) total pressure: 1 bar; (ii) CO_2 partial pressure: 0.1 bar; total pressure: 1 bar (iii) temperature 35 °C; (iv) dosage gas composition 90% He–10% CO_2. [b] Calorimetric conditions: (i) CO_2 partial pressure: 0.1 bar; (ii) temperature 30 °C.

this is the same as the amount originally adsorbed in the sample. In this case it seems very likely that a portion of the amount adsorbed is chemically bound to the amine groups, therefore irreversibly adsorbed during the time of the experiment. Temperature programmed desorption (TPD) was carried out on some of the samples, but the signal related to the amount desorbed at high temperature was too close to the detector baseline to be accurately quantified. This, together with the difference in temperature between the two experiments, explains the small discrepancy with the adsorbed amount measured at 25 °C in the volumetric system. The amount adsorbed for the samples is particularly low under these conditions and as a result the experimental ZLC curves are too close to the blank curves. This unfortunately prevents any further analysis on the equilibrium and the kinetics of adsorption.

For carbon capture applications fast adsorption cycles (seconds or minutes) are desirable to achieve high productivity, it is then important to evaluate the performance of novel adsorbents under conditions representative of the real application. For this reason, in this study each ZLC test was carried out for not more than 1 hour in total (adsorption and desorption).

Conclusions

The adsorption properties of SBA-15, prepared both *via* one-pot synthesis and grafted post synthesis with APTS, EAPTS and PAPTS, were studied using a multidisciplinary approach. Both infrared spectroscopy and solid-state NMR of the adsorbed carbon dioxide provided information on the interactions between CO_2 and the basic group of the functionalized silica samples. These techniques confirmed the formation of carbamate species, as a result of chemical interactions between basic amino groups and carbon dioxide. Both FT-IR spectroscopy and SS-NMR spectroscopy suggested that increasing the number of amino groups in the chain, *i.e.* passing from the A-SBA-15 to P-SBA-15 sample, increases also the reactivity toward CO_2. Nevertheless, the samples prepared *via* a post-synthesis grafting procedure, are more reactive towards CO_2 with respect one-pot synthesized ones due to the fact that for these last samples the preparation step under acid conditions led to the protonation of amino groups.

A deeper analysis of the most reactive post-grafted samples was carried out. ^{1}H Hahn echo MAS NMR spectroscopy suggested that A-SBA-15 and P-SBA-15 samples display a similar amount of mobile and rigid components, while E-SBA-15 shows only rigid components. This behavior agrees with the results of *ab initio* modeling: the optimized adducts of the three organosilanes on some silica cluster models show that the APTS chain interacts loosely with the surface, as well as PAPTS when the density of the grafted molecules is high enough. In addition, after the introduction of $^{13}CO_2$, an increase in the rigid part was clearly observed for all the samples.

Finally, for the first time, the amount of adsorbed carbon dioxide on SBA-15 grafted with amino-silanes was estimated comparing two different quantitative techniques: a classical microcalorimetric analysis and Zero Length Column chromatography. In particular, the obtained values of the CO_2 adsorption capacity by means of microcalorimetry are 0.31, 0.51 and 0.68 mol kg^{-1}, respectively, for A-SBA-15, E-SBA-15 and P-SBA-15, while the CO_2 adsorption capacity values obtained with ZLC are 0.21, 0.44 and 0.53 mol kg^{-1}, respectively, for A-SBA-15, E-SBA-15 and P-SBA-15.

Acknowledgements

The financial support of the PRIN Project no. 2010A2FSS9 entitled: "Mechanisms of CO_2 activation for the design of new materials for energy and resource efficiency" is gratefully acknowledged.

Notes and references

1 B. Li, Y. Duan, D. Luebke and B. Morreale, *Appl. Energy*, 2013, **102**, 1439–1447.
2 S. Y. Lee and S. Y. Park, *J. Ind. Eng. Chem.*, 2015, **23**, 1–11.
3 Q. Wang, L. Luo, Z. Zhong and A. Borgna, *Energy Environ. Sci.*, 2011, **4**, 42–55.
4 J. Wang, L. Huang, R. Yang, Z. Zhang, J. Wu, Y. Gao, Q. Wang, D. O'Hareb and Z. Zhong, *Energy Environ. Sci.*, 2014, **7**, 3478–3518.
5 A. Samanta, A. Zhao, G. K. H. Shimizu, P. Sarkar and P. Gupta, *Ind. Eng. Chem. Res.*, 2012, **51**(13), 1438–1463.
6 J. Tang, J. Liu, N. L. Torad, T. Kimura and Y. Yamauchi, *Nano Today*, 2014, **9**(3), 305–323.
7 K. C. Wu and Y. Yamauchi, *J. Mater. Chem.*, 2012, **22**, 1251–1256.
8 V. Malgras, H. Ataee-Esfahani, H. Wang, B. Jiang, C. Li, K. C.-W. Wu, J. H. Kim and Y. Yamauchi, *Adv. Mater.*, 2016, **28**(6), 993–1010.
9 V. Malgras, Q. Ji, Y. Kamachi T. Mori, F.-K. Shieh, K. C. W. Wu, K. Ariga and Y. Yamauchi, *Bull. Chem. Soc. Jpn.*, 2015, **88**, 1171–1200.
10 C. H. Yu, C. H. Huang and C. S. Tan, *Aerosol Air Qual. Res.*, 2012, **12**, 745–769.
11 C. Chen, J. Kim and W. S. Ahn, *Korean J. Chem. Eng.*, 2014, **31**, 1919–1934.
12 M. Caplow, *J. Am. Chem. Soc.*, 1968, **90**, 6795–6803.
13 B. Dutcher, M. Fan and A. G. Russell, *ACS Appl. Mater. Interfaces*, 2015, **7**, 2137–2148.
14 A. Sayari, A. Heydari-Gorji and Y. Yang, *J. Am. Chem. Soc.*, 2012, **134**, 13834–13842.
15 C. Y. Yoo, L. C. Lee and C. W. Jones, *Langmuir*, 2015, **31**, 13350–13360.
16 V. Zelenák, M. Badanicová, D. Halamová, J. Cejka, A. Zukal, N. Murafa and G. Goerigk, *Chem. Eng. J.*, 2008, **144**, 336–347.
17 X. Yan, L. Zhang, Y. Zhang, Y. Yang and Z. Yan, *Ind. Eng. Chem. Res.*, 2011, **50**, 3220–3226.
18 F. Y. Chang, K. J. Chao, H. H. Cheng and C. S. Tan, *Sep. Purif. Technol.*, 2009, **70**, 87–95.
19 Y. Li, X. Wen, L. Li, F. Wang, N. Zhao, F. Xiao, W. Wei and Y. Sun, *J. Sol–Gel Sci. Technol.*, 2013, **66**, 353–362.

20 D. Zhao, Q. Huo, J. Feng, B. F. Chmelka and G. D. Stucky, *J. Am. Chem. Soc.*, 1998, **120**, 6024–6030.
21 L. Etgar, G. Schuchardt, D. Costenaro, F. Carniato, C. Bisio, S. M. Zakeeruddin, M. K. Nazeeruddin, L. Marchese and M. Graetzel, *J. Mater. Chem. A*, 2013, **1**(39), 10142–10147.
22 S. Hao, H. Chang, Q. Xiao, Y. Zhong and W. Zhu, *J. Phys. Chem. C*, 2011, **115**, 12873–12882.
23 D. Massiot, F. Fayon, M. Capron, I. King, S. Le Calve, B. Alonso, J. O. Durand, B. Bujoli, Z. Gan and G. Hoatson, *Magn. Reson. Chem.*, 2002, **40**, 70–75.
24 M. Eic and D. M. Ruthven, *Zeolites*, 1988, **8**, 40–45.
25 X. Hu, S. Brandani, A. I. Benin and R. R. Willis, *Ind. Eng. Chem. Res.*, 2015, **54**, 6772–6780.
26 J. A. A. Gibson, E. Mangano, E. Shiko, A. G. Greenaway, A. V. Gromov, M. Lozinska, D. Friedrich, E. E. B. Campbell, P. A. Wright and S. Brandani, *Ind. Eng. Chem. Res.*, 2016, **55**, 3840–3851.
27 S. Brandani and D. M. Ruthven, *Adsorption*, 1996, **2**, 133–143.
28 V. Bolis, C. Busco, V. Aina, C. Morterra and P. Ugliengo, *J. Phys. Chem. C*, 2008, **112**(43), 16879–16892.
29 A. D. Becke, *Phys. Rev. B: Condens. Matter Mater. Phys.*, 1988, **38**, 3098–3105.
30 C. Lee, W. Yang and R. G. Parr, *Phys. Rev. B: Condens. Matter Mater. Phys.*, 1988, **37**, 785–791.
31 A. D. Becke, *J. Chem. Phys.*, 1993, **98**, 1372–1381.
32 T. H. Dunning, *J. Chem. Phys.*, 1989, **90**, 1007–1010.
33 R. A. Kendall, T. H. Dunning and R. J. Harrison, *J. Chem. Phys.*, 1992, **96**, 6796–6801.
34 P. J. Hay and W. R. Wadt, *J. Chem. Phys.*, 1985, **82**, 270–279.
35 T. Schwabe and S. Grimme, *Phys. Chem. Chem. Phys.*, 2006, **8**, 4398–4404.
36 P. Ugliengo, M. Sodupe, F. Musso, I. J. Bush, R. Orlando and R. Dovesi, *Adv. Mater.*, 2008, **20**, 4579–4583.
37 J. M. R. Gallo, C. Bisio, G. Gatti, L. Marchese and H. O. Pastore, *Langmuir*, 2010, **26**, 5791–5800.
38 S. Lowell, J. E. Shields, M. A. Thomas and M. Thommes, *Characterization of Porous Solids and Powders: Surface Area, Pore Size and Density*, Kluwer Academic Publishers, 2004.
39 F. Hoffmann, M. Cornelius, J. Morell and M. Fröba, *Angew. Chem., Int. Ed.*, 2006, **45**, 3216–3225.
40 M. Thommes, K. Kaneko, A. V. Neimark, J. P. Olivier, F. Rodriguez-Reinoso, J. Rouquerol and K. S. W. Sing, *Pure Appl. Chem.*, 2015, **87**(9-10), 1051–1069.
41 M. Kruk and M. Jaroniec, *Chem. Mater.*, 2000, **12**, 1961–1968.
42 F. Cucinotta, F. Carniato, G. Paul, S. Bracco, C. Bisio, S. Caldarelli and L. Marchese, *Chem. Mater.*, 2011, **23**(11), 2803–2809.
43 M. W. Hahn, M. Steib, A. Jentys and J. A. Lercher, *J. Phys. Chem. C*, 2015, **119**, 4126–4135.
44 Z. F. Tran, D. Busche, B. Fryxell, L. Addleman, R. Zemanian, T. Aardahl and L. Christopher, *Ind. Eng. Chem. Res.*, 2005, **44**, 3099–3105.
45 G. Socrates, *Infrared Characteristic Group Frequencies*, John Wiley & Sons, Ltd, 2001.
46 C. Knofel, C. Martin, V. Hornebecq and P. L. Llewellyn, *J. Phys. Chem. C*, 2009, **113**, 21726–21734.
47 X. Wang, W. Schwartz, J. C. Clark, X. Ma, S. H. Overbury, X. Xu and C. Song, *J. Phys. Chem. C*, 2009, **113**, 7260–7268.
48 H. Y. Huang, R. T. Yang, D. Chinn and C. L. Munson, *Ind. Eng. Chem. Res.*, 2003, **42**, 2427–2433.
49 S. Hao, H. Chang, Q. Xiao, Y. Zhong and W. Zhu, *J. Phys. Chem. C*, 2011, **115**, 12873–12882.
50 Z. Bacsik, R. Atluri, A. E. Garcia-Bennett and N. Hedin, *Langmuir*, 2010, **26**, 10013–10024.
51 N. Hiyoshi, K. Yogo and T. Yashima, *Chem. Lett.*, 2004, **33**, 510–511.
52 A. Danon, P. C. Stair and E. Weitz, *J. Phys. Chem. C*, 2011, **115**, 11540–11549.
53 O. Leal, C. Bolivar, C. Ovalles and J. J. Garcia, *Inorg. Chim. Acta*, 1995, **240**, 183–189.
54 M. L. Pinto, L. Mafra, J. M. Guil, J. Pires and J. Rocha, *Chem. Mater.*, 2011, **23**, 1387–1395.
55 J. K. Moore, M. A. Sakwa-Novak, W. Chaikittisilp, A. K. Mehta, M. S. Conradi, C. W. Jones and S. E. Hayes, *Environ. Sci. Technol.*, 2015, **49**, 13684–13691.
56 N. Hiyoshi, K. Yogo and T. Yashima, *Microporous Mesoporous Mater.*, 2005, **84**, 357.
57 F. Zheng, D. Tran, B. Busche, G. Fryxell, R. Shane Addleman, T. Zemanian and C. Aardahl, *Ind. Eng. Chem. Res.*, 2005, **44**, 3099.
58 C. Knofel, J. Descarpentries, A. Banzaouia, V. Zelenak, S. Mornet, P. L. Llewellyn and V. Hornebecq, *Microporous Mesoporous Mater.*, 2007, **99**, 79–85.
59 C. Knofel, C. Martin, V. Hornebecq and P. L. Llewellyn, *J. Phys. Chem. C*, 2009, **113**, 21726–21734.
60 F. Brandani, D. M. Ruthven and C. G. Coe, *Ind. Eng. Chem. Res.*, 2003, **42**, 1451–1461.

